Radiology

Dynamic Contrast-enhanced MR Imaging of Advanced Hepatocellular Carcinoma: Comparison with the Liver Parenchyma and Correlation with the Survival of Patients Receiving Systemic Therapy[1]

Bang-Bin Chen, MD
Chao-Yu Hsu, MD
Chih-Wei Yu, MD
Po-Chin Liang, MD
Chiun Hsu, PhD
Chih-Hung Hsu, PhD
Ann-Lii Cheng, PhD
Tiffany Ting-Fang Shih, MD

Purpose: To retrospectively compare the perfusion parameters of advanced hepatocellular carcinoma (HCC) measured with dynamic contrast material–enhanced (DCE) magnetic resonance (MR) imaging with surrounding liver parenchyma to determine the relationship between these parameters and uncensored overall survival (OS).

Materials and Methods: This retrospective study had institutional review board approval, and informed consent was waived. DCE MR imaging was performed in 92 patients with advanced HCC before systemic treatment was administered (19 patients received a placebo). Three semiquantitative (peak, slope, and area under the gadolinium concentration-time curve [AUC]) and six quantitative (arterial fraction, arterial flow, portal flow, total blood flow, distribution volume, and mean transit time) parameters were calculated by placing regions of interest in the largest area of the tumor and background liver parenchyma. The DCE MR imaging parameters between the tumor and normal liver were compared with paired Wilcoxon test. By using the Cox proportional hazards model for univariate and multivariate analyses, the association of DCE MR imaging parameters and OS was investigated.

Results: HCC demonstrated significantly higher peak, slope, AUC, arterial fraction, and arterial flow but lower portal flow, distribution volume, and mean transit time than did the background liver (all $P < .05$). Patients with high peak in the tumor had longer OS ($P = .005$) than did those with low peak. Cox multivariate analysis identified peak as an independent predictor of OS ($P = .032$) after adjusting for age, sex, treatment, tumor size, and portal vein thrombosis.

Conclusion: DCE MR imaging parameters can be used to differentiate advanced HCC from the background liver, and peak, a semiquantitative parameter, is associated with outcome in patients with advanced HCC before systemic therapy.

An earlier incorrect version of this article appeared online. This article was corrected on July 22, 2016.

[1] From the Department of Medical Imaging and Radiology (B.B.C., C.Y.H., C.W.Y., P.C.L.) and Department of Oncology (C.H., C.H.H., A.L.C.), National Taiwan University College of Medicine and Hospital, Taipei, Taiwan; Department of Radiology (C.Y.H.), Taipei Hospital, Ministry of Health and Welfare, New Taipei, Taiwan; and Department of Medical Imaging, Taipei City Hospital, No 7 Chung-Shan South Rd, Taipei 10016, Taiwan (T.T.F.S.). Received December 2, 2015; revision requested January 7, 2016 and received January 31; accepted February 19; final version accepted February 24. **Address correspondence to** T.T.F.S. (e-mail: *ttfshih@ntu.edu.tw*).

Supported by the Ministry of Science and Technology, Executive Yuan, ROC, Taiwan (NSC 100-2314-B-002-053 and National Taiwan University Hospital (NTUH 101-001863).

Hepatocellular carcinoma (HCC) is the sixth most common cancer worldwide (1). Curative or local-regional therapies are recommended for patients with early- or intermediate-stage HCC (2). Sorafenib, the only systemic therapeutic drug approved for advanced HCC by the Food and Drug Administration, has antiproliferative and antiangiogenic properties (3,4). The relative success of sorafenib therapy has engendered an increased interest in developing and testing other targeted molecular medications. Most of the other drugs—including vandetanib, sunitinib, brivanib, and linifanib—that are currently being developed to treat patients with HCC also target tumor angiogenesis as the major antitumor mechanism (5–8).

Dynamic contrast material–enhanced (DCE) magnetic resonance (MR) imaging is a technique used to measure the perfusion, blood flow, and vascularity of tissue by analyzing the signal enhancement curve of tissue. Microscopically, the parameters derived from DCE MR imaging (such as forward volume transfer constant [K^{trans}]) are correlated with tumor microvessel density and vascular endothelial growth factor (VEGF) expression (9–13). Therefore, DCE MR imaging can be used to reliably depict and quantify the suppression of tumor vascular permeability induced by antiangiogenic agents. In many current clinical trials for new antiangiogenic agents, DCE MR imaging was used as an early imaging biomarker to evaluate patients' response to treatment (14–16).

This signal enhancement of liver or tumor perfusion can be quantified with semiquantitative or quantitative analysis (10,17,18). Semiquantitative analysis is performed by calculating heuristic parameters, which can be extracted from signal intensity curves. In contrast, quantitative analysis requires computation-based curve-fitting algorithms, which are obtained by using a compartment model with an arterial input function (19–21). Such quantitative parameters are correlated with tumor angiogenesis and liver fibrosis severity (11,14,22,23). The quantitative parameters have also been used to evaluate perfusion differences between HCC and the background liver and between HCC and colorectal hepatic metastases (20,24). Data regarding the correlation between the semiquantitative and quantitative DCE MR imaging parameters in HCC remain unknown, although a substantial correlation between these parameters was revealed in breast cancer (25).

DCE MR imaging can be used to predict clinical responses to antiangiogenic treatment and survival in patients with HCC (26,27). To our knowledge, data regarding the use of pretreatment DCE MR imaging parameters to predict outcome in patients with HCC after systemic therapy remain limited. Therefore, the purpose of this study was to retrospectively compare the perfusion parameters of advanced HCC that were measured with DCE MR imaging with the surrounding liver parenchyma to determine the relationship between these parameters and uncensored overall survival (OS).

Advances in Knowledge

- In patients with advanced hepatocellular carcinoma (HCC) who are undergoing dynamic contrast-enhanced MR imaging, peak and area under the gadolinium concentration-time curve (AUC) were significantly correlated with all fully quantitative parameters (arterial, portal and total blood flow, arterial fraction, distribution volume, mean transit time, forward volume transfer constant, reverse volume transfer constant, and extravascular extracellular space volume per unit volume of tissue; $P < .05$), and slope was significantly correlated with total blood flow ($P < .05$).
- HCC had significantly higher peak, slope, AUC, arterial fraction, and arterial flow but lower portal blood flow, distribution volume, and mean transit time than did the background liver (all $P < .05$).
- Tumors with large portal vein thrombosis exhibited lower peak ($P = .041$) and slope ($P = .017$) than did those without a large portal vein thrombosis.
- Cox multivariate analysis identified peak as an independent predictor of overall survival ($P = .032$) after adjusting for age, sex, treatment, tumor size, and portal vein thrombosis.

Implication for Patient Care

- Dynamic contrast-enhanced MR imaging may potentially be used to predict survival in patients with advanced HCC before they undergo systemic therapy and help clinicians select patients who can benefit from therapy.

Materials and Methods

Patients

This retrospective study was approved by the Research Ethics Committee of National Taiwan University Hospital,

Published online before print
10.1148/radiol.2016152659 **Content codes:** GI MR

Radiology 2016; 281:454–464

Abbreviations:
AF = absolute arterial liver blood flow
AUC = area under the gadolinium concentration-time curve
DCE = dynamic contrast enhanced
HCC = hepatocellular carcinoma
K^{trans} = forward volume transfer constant
MTT = mean transit time
OS = overall survival
PF = absolute portal liver blood flow
PVT = portal vein thrombosis
ROI = region of interest
TF = absolute total liver blood flow
VEGF = vascular endothelial growth factor

Author contributions:
Guarantors of integrity of entire study, B.B.C., C.Y.H., P.C.L., T.T.F.S.; study concepts/study design or data acquisition or data analysis/interpretation, all authors; manuscript drafting or manuscript revision for important intellectual content, all authors; approval of final version of submitted manuscript, all authors; agrees to ensure any questions related to the work are appropriately resolved, all authors; literature research, B.B.C., C.Y.H., C.W.Y., P.C.L., T.T.F.S.; clinical studies, all authors; experimental studies, C.W.Y., P.C.L.; statistical analysis, B.B.C., P.C.L., C.H., T.T.F.S.; and manuscript editing, B.B.C., C.Y.H., P.C.L., C.H., C.H.H., T.T.F.S.

Conflicts of interest are listed at the end of this article.

and informed consent was waived. We evaluated the DCE MR imaging parameters of advanced HCC and survival outcomes from two prospective phase II clinical trials (5,26). All patients provided informed consent for these two clinical trials. From August 2007 to April 2009, 92 patients with advanced HCC agreed to undergo DCE MR imaging before target or systemic therapy. The characteristics of these patients were consistent with typical epidemiologic features of HCC in Taiwan (Table 1) (28). Data for all 92 patients were reported in previous studies (5,26), which focused on the correlation of a single DCE MR imaging parameter (K^{trans}), with different treatment groups or survival. By contrast, in this study, we reported on the correlation of 12 DCE MR imaging parameters with survival. Of the 92 study patients, 54 entered into a phase II clinical trial for vandetanib therapy (vandetanib, n = 35; placebo, n = 19; registered with ClinicalTrials.gov [NCT00508001]) and 38 entered into another phase II clinical trial for sorafenib and tegafur or uracil therapy (registered with ClinicalTrials.gov [NCT00464919]) (5,26). In the clinical trial for vandetanib therapy, two DCE MR imaging examinations (performed at baseline and 7 days) were mandatory. In the clinical trials for sorafenib and tegafur or uracil therapy, three DCE MR imaging examinations (performed at baseline and days 3 and 14) were optional. In the present study, we only analyzed baseline MR images. Vandetanib targets both VEGF receptor and epidermal growth factor receptor signaling pathways. Sorafenib is a multitarget kinase inhibitor that targets both rapidly accelerated fibrosarcoma and VEGF receptor kinases.

The following major inclusion criteria were used: *(a)* advanced HCC not amenable to local-regional therapy, *(b)* at least one measurable tumor according to the Response Evaluation Criteria in Solid Tumors, and *(c)* adequate organ function reserves (5,26). Treatment was continued until the tumor progressed or unacceptable toxicity developed. We divided the 92 patients into the following three groups according to the treatment they received: in group 1 (n = 35), patients received 100 or 300 mg of vandetanib therapy; in group 2 (n = 38), patients received sorafenib plus tegafur or uracil therapy; and in group 3 (n = 19), patients received a placebo.

Outcome Endpoints

Overall mortality was determined from the Taiwan National Health Insurance Research Database or hospital electronic medical records. OS was measured from the date of DCE MR imaging to the date of death.

DCE MR Imaging Protocol

All DCE MR images were obtained with a 1.5-T superconducting magnet (Magnetom Sonata; Siemens Medical Solutions, Erlangen, Germany) and a phased-array body coil. First, two-point localizers were placed on the largest area of the index tumor and the abdominal aorta to define an oblique coronal plane that could cover most of the tumor and abdominal aorta. A dose of 0.15 mmol/kg of gadodiamide (Omniscan; GE Amersham, Oslo, Norway) was injected into an antecubital vein with an automated injector at a rate of 4 mL/sec and followed by a 20-mL saline flush. Baseline images were acquired 10 seconds (10 phases) before initiating contrast agent injection. DCE MR imaging was performed at five continuous oblique coronal sections, with breath-holding, a T1-weighted two-dimensional fast spoiled gradient-echo sequence, and the following parameters: section thickness, 8 mm; section gap, 2 mm; repetition time msec/echo time msec, 200/1.0; flip angle, 18°; field of view, 320 × 360 mm; matrix size, 224 × 256. All patients were asked to hold their breath for as long as they could tolerate and to then breathe slowly and smoothly during imaging. The total acquisition time for DCE MR images was 110 seconds, with 550 dynamic images obtained in each patient. Finally, a static contrast-enhanced T1-weighted fat-suppressed spin-echo sequence (section thickness, 6 mm; section gap, 1.5 mm; 130/4.8; flip angle, 70°; field of view, 360 × 293 mm; matrix size, 512 × 416) was performed in the same oblique coronal plane to image the entire liver. All imaging was performed by the same technician.

Table 1

Demographics and Clinical Characteristics of 92 Patients with Advanced HCC

Characteristic	Measure
Age (y)*	55.8 ± 11.9 (23–83)
Sex	
Male	77 (84)
Female	15 (16)
Child-Pugh stage	
A	92 (100)
B	0 (0)
Viral cause	
Hepatitis B infection	65 (71)
Hepatitis C infection	12 (13)
Hepatitis B and C infection	4 (4)
Neither hepatitis B nor C infection	11 (12)
Previous treatment	38 (41)
Surgery	16 (17)
Radiofrequency ablation	5 (5)
TACE	30 (33)
ECOG performance status	
0	28 (30)
1	63 (68)
2	1 (1)
BCLC stage	
B	10 (11)
C	82
Tumor size (cm^2)*	60.3 ± 59.3 (12.1–96)
Tumor location	
Right lobe	39 (42)
Left lobe	12 (13)
Both lobes	41 (45)
Extrahepatic metastasis	61 (66)
PVT	
Main	25 (27)
Lobar	20 (22)
Segmental	17 (18)
Not present	30 (33)

Note.—Unless otherwise indicated, data are numbers of patients, and data in parentheses are percentages. BCLC = Barcelona Clinic Liver Cancer, ECOG = Eastern Cooperative Oncology Group, TACE = transarterial chemoembolization.

* Data are mean plus or minus standard deviation, and data in parentheses are the range.

Image Analysis

Postprocessing of all DCE MR imaging data was performed with a commercial software tool (MIStars; Apollo Medical Imaging, Melbourne, Australia). During the image coregistration phase, movement corrections were manually performed by an experienced radiologist (C.B.B., with 10 years of experience in abdominal DCE MR imaging).

Regions of interest (ROIs) were manually drawn on the main portal vein at the level of the porta hepatis, proximal abdominal aorta at the level of the celiac axis, HCC, and background liver tissue (at least 3 cm away from HCC lesions) to measure signal intensity values. ROIs on the aorta and portal vein were used for the arterial input function. The aorta and liver ROIs were drawn for a single time frame, transferred to the remaining time frames, and then manually corrected if required. All ROIs were drawn by the same radiologist (C.B.B.), who was blinded to patients' clinical data. The mean ROI in the tumor was 60.3 cm^2 ± 59.3 (range, 12.1–96 cm^2). The fixed ROI area in the liver parenchyma was 3 cm^2, with avoidance of large vascular structures or liver lesions.

Curve Analysis Method and Dual-Input Single-Compartment Model for Background Liver Parenchyma and HCC

In DCE MR imaging, a linear relationship was assumed between signal intensity values and the gadolinium concentration for the range of expected concentrations in the liver (0.0–0.5 mM/L) and blood (0–5 mM/L). Therefore, our conversion was based on the following approximation, (29):

$$C = k(S - S0)/S0,$$

where C is tissue tracer concentration, $S0$ is the unenhanced signal intensity, S is the contrast-enhanced signal intensity, and k is the scaling constant (0.395 for the liver and 0.201 for blood). These constants are based on a prior phantom and human calibration study (30).

For the curve analysis method, the following semiquantitative parameters were obtained by analyzing the characteristics of the hepatic or tumor enhancement curves: peak (maximal signal intensity minus baseline signal intensity), slope (maximal ascending slope of the curve), and initial area under the gadolinium concentration-time curve (AUC) over 100 seconds (measured in millimoles per second). This method does not depend on the record of the arterial or portovenous input function (23).

We then used a dual-input single-compartment pharmacokinetic model to extract microcirculatory quantitative parameters from raw data. This model comprises the dual blood supply from the portal vein and hepatic artery received by the liver and considers the liver parenchyma or tumor as a single compartment (20,31,32).

The following parameters were obtained: arterial fraction, which is measured as a percentage; absolute arterial liver blood flow (AF), which is measured in milliliters per 100 g/m; absolute portal liver blood flow (PF), which is measured in milliliters per 100 g/m; absolute total liver blood flow (TF), which is measured in milliliters per 100 g/m; distribution volume, which is measured as a percentage; and mean transit time (MTT), which is measured in seconds. Distribution volume indicates the total volume of contrast agent in the liver compartment. MTT is the average time for the contrast agent to pass through the liver compartment from the arterial or portal venous input to the hepatic vein (31). The tissue tracer concentration *(C)* was estimated by empirically determining the relationship between signal intensity and T1 values according to the pulse sequence used (29–31).

Single-Input Two-Compartment Model for HCC

Because HCC typically manifests with an exclusive or near-exclusive arterial supply, we also used a single-input two-compartment model for pharmacokinetic modeling in HCC: forward volume transfer constant (K^{trans}; measured in m^{-1}), reverse volume transfer constant (measured in m^{-1}), and extravascular extracellular space volume per unit volume of tissue (measured as a percentage) (21). These parameters were automatically calculated pixel by pixel by using a constrained nonlinear least-squares fitting algorithm with adjustable delay time. For K^{trans}, in addition to a whole-tumor ROI, a 1-cm^2 ROI in the most contrast-enhanced tumor region was measured to correlate with OS (26).

Statistical Analyses

The estimated semiquantitative and quantitative parameters were compared between HCC and the background liver by using the Wilcoxon signed-rank test because the parameters did not follow a normal distribution. Student t test was used to compare the perfusion parameters in HCC without and with large portal vein thrombosis (PVT). Pearson correlation *(r)* was used to determine the correlations among various DCE MR imaging parameters. Survival is presented as Kaplan-Meir survival curves, with the analysis performed with the Mantel-Cox log-rank test. The median values of DCE MR imaging parameters were used as cut-off values. Age, sex, treatment group, tumor size, Eastern Cooperative Oncology Group performance status, Barcelona Clinic Liver Cancer stage, PVT, and DCE MR imaging parameters were included in the univariate Cox regression models for OS. Variables with P values $< .05$ at univariate analysis were used as input variables for a multivariate model. All statistical analyses were performed with statistical software (SPSS for Windows 22; SPSS, Chicago, Ill). $P < .05$ was considered to indicate a significant difference. Bonferroni correction was applied to adjust for multiple comparisons ($P < .006$).

Results

Comparison of DCE MR Imaging Parameters between HCC and Background Liver

Regarding the semiquantitative parameters, all values were significantly higher in HCC than in the background liver ($P < .05$). Slope and AUC were still significant after Bonferroni correction

($P < .006$) was performed. For the quantitative parameters, HCC had higher arterial fraction and AF, but lower PF, distribution volume, and MTT than the background liver (all $P < .05$). Moreover, arterial fraction, AF, PF, and distribution volume became significant after Bonferroni correction ($P < .006$) was performed. No significant differences were observed in TF (Table 2).

Table 2

Comparison of DCE MR Imaging Parameters between HCC and Background Liver

Parameter	Background Liver	HCC	*P* Value
Curve analysis method			
Peak	289.0 (116.7)	314.4 (123.3)	.034*
Slope	78.2 (38.3)	102.1 (50.8)	<.001*†
AUC	1667.1 (752.1)	1932.7 (858.6)	.002*†
Dual-input one compartment			
Arterial fraction (%)	29.6 (27.3)	54.1 (19.8)	<.001*†
AF (mL/100 g/min)	51.9 (66.6)	106.7 (127.8)	<.001*†
PF (mL/100 g/min)	134.4 (101.4)	79.9 (95.6)	<.001*†
TF (mL/100 g/min)	187.9 (115.8)	190.5 (186.7)	.353
Distribution volume (%)	28.3 (23.9)	24.5 (9.1)	<.001*†
MTT (sec)	12.6 (6.1)	11.2 (5.9)	.01*

Note.—Unless otherwise indicated, data are the mean, and data in parentheses are the standard deviation. Statistical analysis was performed with the Wilcoxon signed-rank test.

* $P < .05$.

† After Bonferroni correction, $P < .006$.

Pearson Correlation Between Semiquantitative and Quantitative Parameters in HCC

Peak and AUC were significantly correlated with all fully quantitative parameters (arterial, portal, and total blood flows; arterial fraction; distribution volume; MTT, K^{trans}; reverse volume transfer constant; and extravascular extracellular space volume per unit volume of tissue; all $P < .05$) (Fig 1). Slope was significantly correlated with TF ($r = 0.216$, 95% confidence interval: 0.26, 0.43; $P < .05$) (Table 3).

Effect of Large PVT on DCE MR Imaging Parameters

Large PVT (main or lobar portal veins) was detected in 45 patients (48.9%). Among all DCE MR imaging parameters, tumors with a large PVT exhibited lower peak ($P = .041$) and slope ($P = .017$, nonsignificant after Bonferroni correction) than did those without a PVT. Significant differences were not observed in the other DCE MR imaging parameters (Table 4).

Relationship of OS to DCE MR Imaging Parameters

All patients died by December 2013. The median survival in all patients was 165 days (range, 16–1912 days). Patients who underwent systemic therapy had longer OS than did those who received the placebo (for group 1 vs group 3, median survival = 174 days vs 110 days, $P = .024$; for group 2 vs group 3, median survival = 193 days vs 110 days, $P = .001$), but no difference was observed between the systemic therapy groups (for group 1 vs group 2, median survival = 174 days vs 193 days, $P = .768$) (Fig 2).

Univariate analysis revealed that old age, male sex, use of placebo, large tumor size, and PVT were prognostic factors for poor OS. Among all DCE MR imaging parameters, patients with a high peak before systemic treatment had longer OS than did those with a low peak (median survival, 197 days vs 116 days; hazard ratio, 1.826; 95% confidence interval: 1.193, 2.795; $P = .005$) (Fig 3). Other parameters showed no significant differences in survival (Table 5). Cox multivariate analysis revealed that peak remained an independent predictor of OS (hazard ratio, 1.650; 95% confidence interval: 1.193, 2.795; $P = .032$) after adjusting for age, sex, treatment group, tumor size, and PVT (Table 6).

Discussion

Our results show that both semiquantitative and quantitative DCE MR imaging parameters were effective in distinguishing between advanced HCC and the background liver. The semiquantitative parameters peak and slope were lower in HCCs with PVT than they were in those without PVT. In addition, baseline peak was an independent predictor of OS in patients with HCC before systemic therapy, even after adjusting for age, sex, treatment group, tumor size, and PVT.

HCC is characterized by a highly vascular tumor that develops neovasculature through angiogenesis, during which portal blood flow to the liver parenchyma, which normally provides 70% of the blood supply, decreases. The tumor is mainly supplied by arterial flow, as reflected by increased tumor perfusion caused by blood supply from the hepatic artery (33). Therefore, the perfusion differences between HCC and the background liver may be detected and quantified with DCE MR imaging. Taouli et al (20) reported that HCC has higher arterial fraction and AF and lower distribution volume and PF than does the background liver, with no difference in MTT. Our results are similar to those of Taouli et al, although we observed lower MTT in patients with HCC. The reasons for this discrepancy may be the small sample size ($n = 33$) and early tumor stage in their study; by contrast, the HCCs in our study were more advanced and aggressive. In addition, we observed that both semiquantitative and quantitative DCE MR imaging parameters could be used to differentiate advanced HCCs from the background liver. Furthermore, the color maps generated with DCE MR imaging parameters may help radiologists rapidly identify tumor location and evaluate response to systemic therapy.

Figure 1

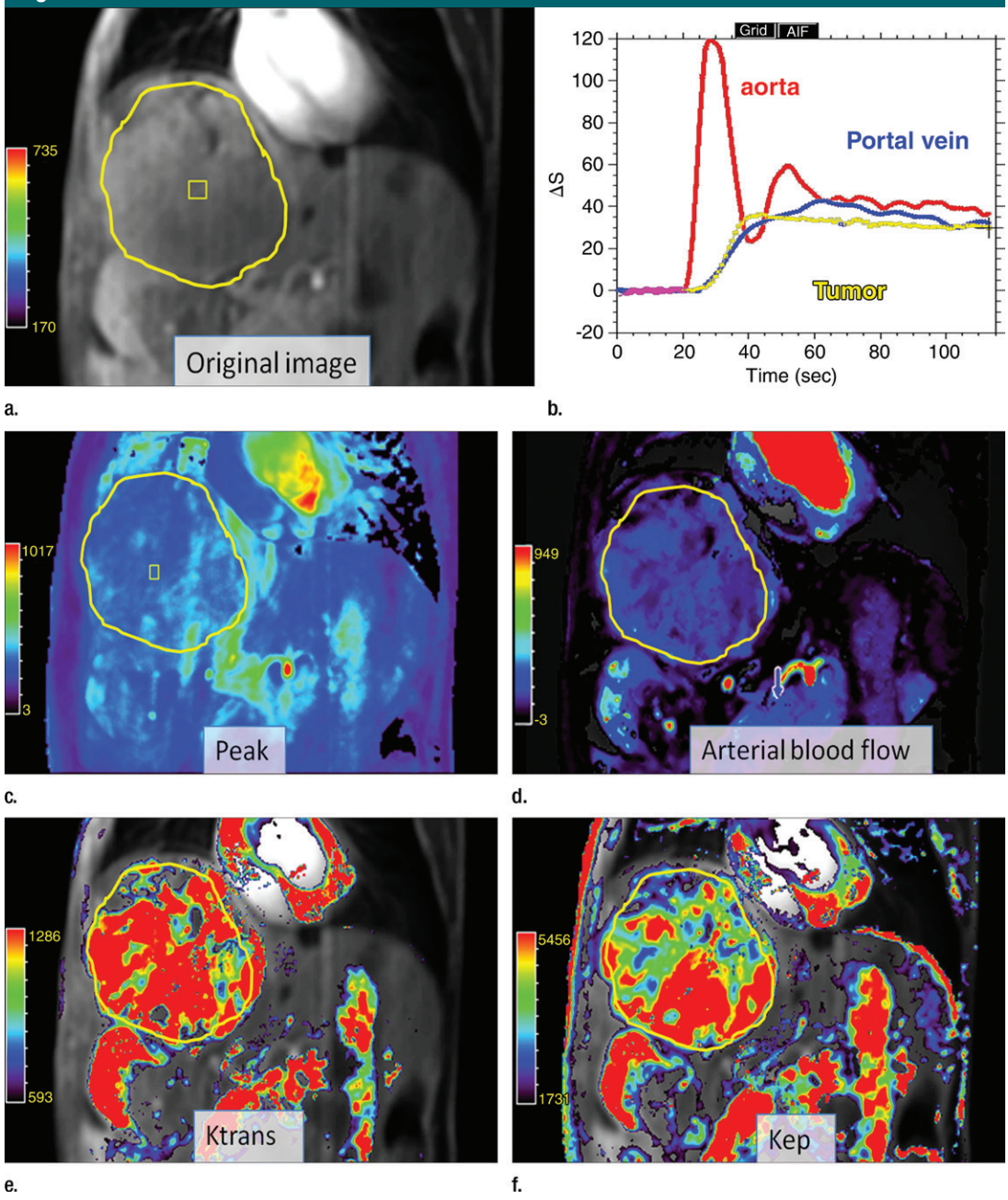

Figure 1: Advanced HCC in a 68-year-old man. **(a)** Contrast-enhanced T1-weighted MR image shows a large tumor in the right upper lobe of the liver. **(b)** Graph shows enhancement curves of the aorta (red line), portal vein (blue line), and tumor (yellow line). **(c–f)** DCE MR images with color maps for **(c)** peak, **(d)** AF (mL/100 g/m), **(e)** K^{trans} (m^{-1}/1000), and **(f)** reverse volume transfer constant (m^{-1}/1000) show that the tumor has increased perfusion, AF, and permeability compared with the background liver.

The advantage of the curve analysis method is its easy calculation; however, the physiologic insights of the descriptive semiquantitative parameters remain unclear (14). By contrast, although measuring model-based parameters is complex, they provide more specific information about true vascular physiology (25). To further understand the physiologic implication of the semiquantitative parameters in HCC, we determined the correlations between semiquantitative and quantitative parameters. Notably, peak and AUC were significantly correlated with

Table 3

Pearson Correlation Analysis between the Semiquantitative and Quantitative Parameters in HCC

Parameter	Peak	Slope	AUC	ART	AF	PF	TF	DV	MTT	K^{trans}	K_{ep}	V_e
Peak	1	0.521*	0.914*	0.286*	0.601*	0.259†	0.574*	0.630*	−0.272*	0.421*	0.236†	0.291*
Slope	…	1	0.349*	−0.009	0.151	0.196	0.216†	0.164	−0.131	0.077	0.039	0.106
AUC	…	…	1	0.322*	0.518*	0.285*	0.517*	0.736*	−0.240†	0.588*	0.425*	0.231†
ART	…	…	…	1	0.425*	−0.434*	0.104	0.077	0.009	0.335*	0.340*	0.008
AF	…	…	…	…	1	0.251†	0.887*	0.376*	−0.508*	0.200	0.068	−0.019
PF	…	…	…	…	…	1	0.656*	0.450*	−0.491*	0.177	0.068	0.124
TF	…	…	…	…	…	…	1	0.488*	−0.627*	0.209†	0.068	0.028
DV	…	…	…	…	…	…	…	1	−0.108	0.638*	0.336*	0.442*
MTT	…	…	…	…	…	…	…	…	1	−0.165	−0.179	0.089
K^{trans}	…	…	…	…	…	…	…	…	…	1	0.840*	0.235†
K_{ep}	…	…	…	…	…	…	…	…	…	…	1	−0.108
V_e	…	…	…	…	…	…	…	…	…	…	…	1

Note.—Data are Pearson correlations. ART = arterial fraction, DV = distribution volume, K_{ep} = reverse volume transfer constant, V_e = extravascular extracellular space volume per unit volume of tissue

* Correlation was significant at the .01 level (two-tailed).

† Correlation was significant at the .05 level (two-tailed).

all fully quantitative parameters. These results suggest that both peak and AUC represent a combination of blood flow, interstitial volume, and permeability. Hence, they may reflect gross angiogenesis within a tumor. In addition, slope was significantly correlated only with total blood flow, so it may be used to estimate total perfusion within a tumor. While fully quantitative DCE MR imaging data are straightforward in concept, acquiring such data is often very time consuming because model fitting must be separately performed for each image voxel. The analysis time cost may become a substantial burden in a fast-paced clinical environment, especially when a patient's dataset contains multiple sections in each image (14). Therefore, the information of these correlations may help in selecting the most satisfactory semiquantitative parameter to represent tumor perfusion, flow, and angiogenesis in daily practice.

Table 4

Comparison of DCE MR Imaging Parameters between HCC without and with Large PVT

	No Large PVT		Large PVT		
Method	Mean	SD	Mean	SD	*P* Value
Curve analysis					
Peak	313.2	114.1	263.7	115.1	.041*
Slope	114.3	60.4	89.4	34.6	.017*
AUC	1770.4	744.7	1559.1	752.7	.179
Dual-input one compartment					
Arterial fraction (%)	55.3	17.6	52.7	21.9	.536
AF (mL/100 g/min)	107.7	117.2	109.3	138.4	.953
PF (mL/100 g/min)	79.0	98.0	85.0	94.2	.768
TF (mL/100 g/min)	186.8	174.0	202.5	202.6	.692
Distribution volume (%)	23.8	8.7	25.7	9.4	.326
MTT (s)	10.5	5.2	11.6	6.4	.387
Single-input two compartments					
K^{trans} (min^{-1}/1000)	489.8	367.9	468.1	354.7	.774
K_{ep} (min^{-1}/1000)	2139.3	1281.5	2021.6	983.7	.622
V_e (%)	26.4	23.7	21.7	9.4	.205

Note.—For no large PVT, $n = 47$, and for large PVT, $n = 45$. Statistical analysis was performed with Student *t* test. Large PVT includes thrombosis in the main or lobar portal veins. No large PVT includes a patent portal vein and thrombosis in the segmental portal vein. Peak and slope were nonsignificant after Bonferroni correction ($P > .006$). K_{ep} = reverse volume transfer constant, SD = standard deviation, V_e = extravascular extracellular space volume per unit volume of tissue.

* $P < .05$.

To our knowledge, the perfusion changes in patients with HCC and PVT have not been adequately investigated in previous studies. In our study, tumors with a large PVT demonstrated lower peak and slope than did those without PVT, although there was some overlap between these two groups. Nevertheless, no significant differences were observed in any quantitative DCE MR imaging parameters. These results indicate that gross perfusion and flow may be lowered in HCC with a large PVT, although HCC receives its main blood supply from the hepatic artery. In addition, in patients with advanced HCCs, semiquantitative DCE MR imaging parameters may more satisfactorily detect PVT-induced perfusion changes than quantitative parameters.

In addition to tumor characterization and treatment response evaluation,

Figure 2

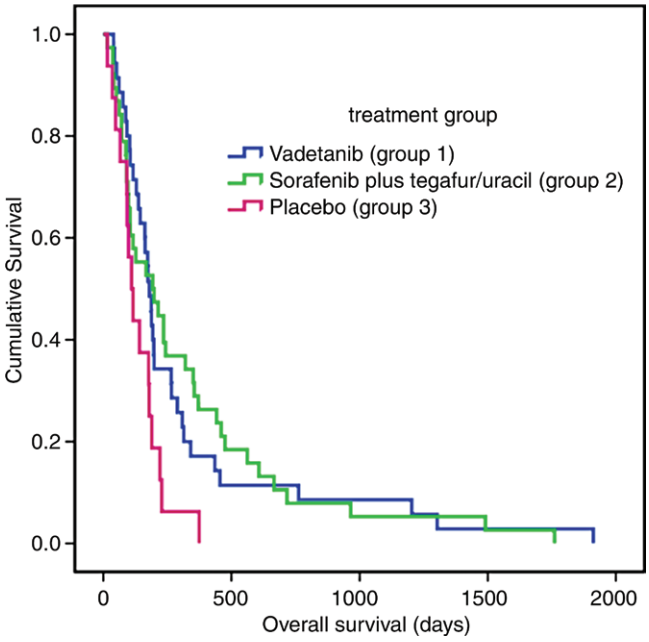

Figure 2: Kaplan-Meier survival curves of the 92 patients in the three treatment groups show that patients who received systemic therapy had longer OS than did those who received the placebo. For group 1 (blue line) versus group 2 (green line), median survival was 174 days and 193 days, respectively, and $P = .024$. For group 2 versus group 3 (red line), median survival was 193 days and 110 days, respectively, and $P = .001$. No difference was observed between the two systemic therapy groups (group 1 vs group 2, median survival = 174 days vs 193 days, $P = .768$).

Figure 3

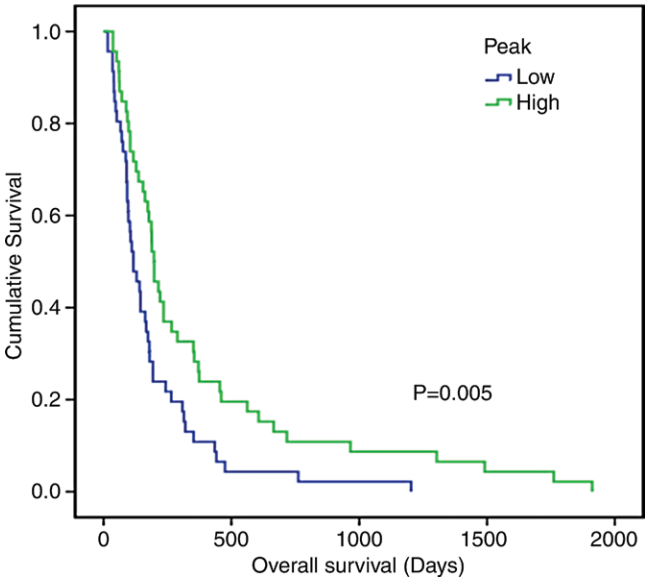

Figure 3: Kaplan-Meier survival curve of peak, a DCE MR imaging parameter, shows that patients with a high peak (green line) before undergoing systemic treatment had longer OS than did those with a low peak (blue line; median survival, 197 days vs 116 days, $P = .005$).

pretreatment DCE MR imaging parameters may be used to predict survival in patients with breast cancer, renal cell cancer, and acute myeloid leukemia (27,34–37). Jarnagin et al (38) determined that a high pretreatment AUC was associated with long median survival in patients with a primary liver tumor (26 patients with intrahepatic cholangiocarcinoma and eight with HCC) who underwent hepatic arterial infusion. Both peak and AUC represent gross angiogenesis within a tumor. Therefore, our result that a high pretreatment peak indicates longer OS (197 days vs 116 days) is consistent with that reported by Jarnagin et al (38). In a prospective study performed in the Asia-Pacific region, median OS was 6.5 months in patients who underwent sorafenib therapy and 4.2 months in those who received a placebo, indicating that the survival difference observed in the current study is also clinically important (4). On the basis of these findings, we hypothesized that patients with high tumor angiogenesis have elevated perfusion parameters and are more likely to respond to the antiangiogenic effects of systemic therapy (39). Such patients should have a more satisfactory survival outcome than those with low tumor angiogenesis (16). Additional studies are required to validate the DCE MR imaging parameters that can be used to monitor vascular changes after local or systemic therapy (14,16,40).

In our previous study of 38 patients with locally advanced HCC who underwent sorafenib and cytotoxic therapy, the baseline K^{trans} that was measured in a 10-pixel operator-defined ROI on the most enhanced tumor region (instead of the whole tumor) was significantly higher in patients with a partial response or stable disease than in those with progressive disease (26). In the present study, we used a whole-tumor ROI and found that only the baseline peak correlated with OS. We also measured a 1-cm^2 ROI in the most contrast-enhanced tumor region in all 92 patients; however, the baseline K^{trans} did not show differences in survival. Hence, peak could be a superior biomarker to K^{trans} for predicting survival. Additional studies are required to standardize ROI measurement and validate the method for response evaluation in these patients. Furthermore, 28 (74%) of the 38 patients included in the analysis died by the end of the previous study (25); by contrast, in our study, all patients died, and OS data were uncensored.

Our study has several limitations. First, our sample size was small, which rendered certain parameters insignificant after Bonferroni correction. In addition, the datasets of two clinical trials were pooled, and 19 patients received the placebo because of the design of the phase II clinical trial of the target therapy. Second, the reproducibility of

Table 5

Factors Associated with OS at Univariate Analysis in 92 Patients

Parameter	HR	95% CI	*P* Value
Age (≥55 vs <55)	1.639	1.067, 2.518	.022*
Sex (male vs female)	2.000	1.126, 3.552	.016*
Treatment			
Vandetanib vs placebo	0.511	0.285, 0.917	.024*
Sorafenib and tegafur or uracil vs placebo	0.454	0.249, 0.827	.001*
Size (<60 cm^2 vs ≥60 cm^2)	0.454	0.289, 0.714	.001*
PVT (no vs yes)	0.591	0.386, 0.904	.014*
BCLC stage (C vs B)	1.322	0.683, 2.559	.407
ECOG performance status (1–2 vs 0)	0.894	0.566, 1.412	.631
Curve analysis method			
Peak	1.826	1.193, 2.795	.005*
Slope	1.169	0.773, 1.767	.458
AUC	1.339	0.885, 2.025	.164
Dual-input one compartment			
Arterial fraction	1.112	0.742, 1.695	.584
AF	1.365	0.895, 2.08	.145
PF	0.853	0.563, 1.294	.453
TF	1.006	0.665, 1.521	.978
Distribution volume	1.222	0.809, 1.846	.338
MTT	1.028	0.677, 1.561	.895
Single-input two compartments			
K^{trans}	1.150	0.756, 1.749	.513
Whole-tumor ROI	1.254	0.823, 1.908	.292
1 cm^2 ROI			
K_{ep}	1.147	0.759, 1.734	.512
V_e	1.103	0.731, 1.665	.641

Note.—BCLC = Barcelona Clinic Liver Cancer, CI = confidence interval, ECOG = Eastern Cooperative Oncology Group, HR = hazard ratio, K_{ep} = reverse volume transfer constant, V_e = extravascular extracellular space volume per unit volume of tissue.

* $P < .05$.

Table 6

Factors Associated with OS at Multivariate Analysis in 92 Patients

Parameter	HR	95% CI	*P* Value
Age (≥55 vs <55 years)	1.197	0.738, 1.942	.466
Sex (male vs female)	1.754	0.973, 3.161	.062
Treatment			
Vandetanib vs placebo	0.549	0.303, 0.995	.048*
Sorafenib and tegafur or uracil vs placebo	0.596	0.329, 1.080	.088
Size (<60 cm^2 vs ≥60 cm^2)	0.544	0.340, 0.872	.011*
PVT (no vs yes)	0.734	0.459, 1.174	.197
Peak (low vs high value)	1.650	1.043, 2.610	.032*

Note.—Peak is dichotomized into high and low values by the median value (265.5). CI = confidence interval, HR = hazard ratio.

* $P < .05$.

DCE MR imaging measurement was not investigated. Previous studies revealed that peak and AUC appear to be the most reproducible among the semiquantitative parameters (10). Although a similar analysis of the reproducibility of semiquantitative and quantitative parameters was reported (41), model-based processing is usually sensitive to noise and arterial input function and, therefore, has lower reproducibility (25). Third, we did not use T1 mapping because it requires perfect motion registration between breath-holding T1 mapping images and free-breathing DCE MR images to accurately calculate quantitative parameters. Most patients had large advanced tumors and could not hold their breath for a long time during DCE MR imaging. Fourth, this was a single-center study, and all measurements were performed by one radiologist who did not assess interobserver or intraobserver variability. Our results must be validated in future multicenter studies. Fifth, our results are based on median values of DCE MR imaging parameters as cut-off values in a particular patient set and would likely yield less significant discrimination or differences in survival estimation in an independent sample of patients.

In conclusion, various DCE MR imaging parameters can be used to quantify perfusion in the liver and HCC. Baseline peak is an independent predictor of OS in patients with HCC who are undergoing systemic therapy, even after adjusting for age, sex, treatment, tumor size, and PVT. Therefore, DCE MR imaging performed before systemic therapy can be used as a noninvasive marker of HCC angiogenesis, and it may be used to predict survival in patients with advanced HCC.

Acknowledgment: All patients included in this study were associated with two other trials (study 1 included 54 patients in a phase II clinical trial with vandetanib and was registered with ClinicalTrials.gov [NCT00508001]; study 2 included 38 patients in a phase II clinical trial with sorafenib and tegafur or uracil and was registered with ClinicalTrials.gov [NCT00464919]) that were conducted by our group. These trials investigated the changes of the single DCE MR imaging parameter K^{trans} on survival outcomes before and after target therapy. The current study focuses on the pretreatment values of various DCE MR imaging parameters on survival outcomes in these patients and on intercorrelation of other semiquantitative and quantitative DCE MR imaging parameters. The results of this study were not previously published.

Disclosures of Conflicts of Interest: B.B.C. disclosed no relevant relationships. **C.Y.H.** disclosed no relevant relationships. **C.W.Y.** disclosed no relevant relationships. **P.C.L.** disclosed no relevant relationships. **C.H.** disclosed no relevant relationships. **C.-H.H.** disclosed no relevant relationships. **A.L.C.** disclosed no relevant relationships. **T.T.F.S.** disclosed no relevant relationships.

References

1. El-Serag HB. Hepatocellular carcinoma. N Engl J Med 2011;365(12):1118–1127.
2. European Association For The Study Of The Liver; European Organisation For Research And Treatment Of Cancer. EASL-EORTC clinical practice guidelines: management of hepatocellular carcinoma. J Hepatol 2012; 56(4):908–943.
3. Llovet JM, Ricci S, Mazzaferro V, et al. Sorafenib in advanced hepatocellular carcinoma. N Engl J Med 2008;359(4):378–390.
4. Cheng AL, Kang YK, Chen Z, et al. Efficacy and safety of sorafenib in patients in the Asia-Pacific region with advanced hepatocellular carcinoma: a phase III randomised, double-blind, placebo-controlled trial. Lancet Oncol 2009;10(1):25–34.
5. Hsu C, Yang TS, Huo TI, et al. Vandetanib in patients with inoperable hepatocellular carcinoma: a phase II, randomized, double-blind, placebo-controlled study. J Hepatol 2012;56(5):1097–1103.
6. Shen YC, Hsu C, Cheng AL. Molecular targeted therapy for advanced hepatocellular carcinoma: current status and future perspectives. J Gastroenterol 2010;45(8):794–807.
7. Sahani DV, Jiang T, Hayano K, et al. Magnetic resonance imaging biomarkers in hepatocellular carcinoma: association with response and circulating biomarkers after sunitinib therapy. J Hematol Oncol 2013;6:51.
8. Kim H, Keene KS, Sarver DB, et al. Quantitative perfusion- and diffusion-weighted magnetic resonance imaging of gastrointestinal cancers treated with multikinase inhibitors: a pilot study. Gastrointest Cancer Res 2014;7(3-4):75–81.
9. Jackson A, O'Connor JP, Parker GJ, Jayson GC. Imaging tumor vascular heterogeneity and angiogenesis using dynamic contrast-enhanced magnetic resonance imaging. Clin Cancer Res 2007;13(12):3449–3459.
10. Miller JC, Pien HH, Sahani D, Sorensen AG, Thrall JH. Imaging angiogenesis: applications and potential for drug development. J Natl Cancer Inst 2005;97(3):172–187.
11. Wang B, Gao ZQ, Yan X. Correlative study of angiogenesis and dynamic contrast-enhanced magnetic resonance imaging features of hepatocellular carcinoma. Acta Radiol 2005;46(4):353–358.
12. Huang SY, Chen BB, Lu HY, et al. Correlation among DCE-MRI measurements of bone marrow angiogenesis, microvessel density, and extramedullary disease in patients with multiple myeloma. Am J Hematol 2012;87(8):837–839.
13. Biomarkers Definitions Working Group. Biomarkers and surrogate endpoints: preferred definitions and conceptual framework. Clin Pharmacol Ther 2001;69(3):89–95.
14. Chen BB, Shih TT. DCE-MRI in hepatocellular carcinoma-clinical and therapeutic image biomarker. World J Gastroenterol 2014;20(12):3125–3134.
15. O'Connor JP, Jackson A, Parker GJ, Roberts C, Jayson GC. Dynamic contrast-enhanced MRI in clinical trials of antivascular therapies. Nat Rev Clin Oncol 2012;9(3):167–177.
16. De Robertis R, Tinazzi Martini P, Demozzi E, et al. Prognostication and response assessment in liver and pancreatic tumors: The new imaging. World J Gastroenterol 2015; 21(22):6794–6808.
17. Khalifa F, Soliman A, El-Baz A, et al. Models and methods for analyzing DCE-MRI: a review. Med Phys 2014;41(12):124301.
18. Thng CH, Koh TS, Collins DJ, Koh DM. Perfusion magnetic resonance imaging of the liver. World J Gastroenterol 2010;16(13): 1598–1609.
19. Annet L, Materne R, Danse E, Jamart J, Horsmans Y, Van Beers BE. Hepatic flow parameters measured with MR imaging and Doppler US: correlations with degree of cirrhosis and portal hypertension. Radiology 2003;229(2):409–414.
20. Taouli B, Johnson RS, Hajdu CH, et al. Hepatocellular carcinoma: perfusion quantification with dynamic contrast-enhanced MRI. AJR Am J Roentgenol 2013;201(4):795–800.
21. Tofts PS, Brix G, Buckley DL, et al. Estimating kinetic parameters from dynamic contrast-enhanced T(1)-weighted MRI of a diffusable tracer: standardized quantities and symbols. J Magn Reson Imaging 1999; 10(3):223–232.
22. Barrett T, Brechbiel M, Bernardo M, Choyke PL. MRI of tumor angiogenesis. J Magn Reson Imaging 2007;26(2):235–249.
23. Chen BB, Hsu CY, Yu CW, et al. Dynamic contrast-enhanced magnetic resonance imaging with Gd-EOB-DTPA for the evaluation of liver fibrosis in chronic hepatitis patients. Eur Radiol 2012;22(1):171–180.
24. Rao SX, Chen CZ, Liu H, Zeng MS, Qu XD. Three-dimensional whole-liver perfusion magnetic resonance imaging in patients with hepatocellular carcinomas and colorectal hepatic metastases. BMC Gastroenterol 2013;13:53.
25. Yi B, Kang DK, Yoon D, et al. Is there any correlation between model-based perfusion parameters and model-free parameters of time-signal intensity curve on dynamic contrast enhanced MRI in breast cancer patients? Eur Radiol 2014;24(5):1089–1096.
26. Hsu CY, Shen YC, Yu CW, et al. Dynamic contrast-enhanced magnetic resonance imaging biomarkers predict survival and response in hepatocellular carcinoma patients treated with sorafenib and metronomic tegafur/uracil. J Hepatol 2011;55(4):858–865.
27. O'Connor JP, Jayson GC. Do imaging biomarkers relate to outcome in patients treated with VEGF inhibitors? Clin Cancer Res 2012;18(24):6588–6598.
28. Chen DS. Hepatocellular carcinoma in Taiwan. Hepatol Res 2007;37(Suppl 2):S101–S105.
29. Jones RA, Easley K, Little SB, Scherz H, Kirsch AJ, Grattan-Smith JD. Dynamic contrast-enhanced MR urography in the evaluation of pediatric hydronephrosis: Part 1, functional assessment. AJR Am J Roentgenol 2005;185(6):1598–1607.
30. Bokacheva L, Rusinek H, Chen Q, et al. Quantitative determination of Gd-DTPA concentration in T1-weighted MR renography studies. Magn Reson Med 2007;57(6):1012–1018.
31. Materne R, Smith AM, Peeters F, et al. Assessment of hepatic perfusion parameters with dynamic MRI. Magn Reson Med 2002;47(1):135–142.
32. Hagiwara M, Rusinek H, Lee VS, et al. Advanced liver fibrosis: diagnosis with 3D whole-liver perfusion MR imaging--initial experience. Radiology 2008;246(3):926–934.
33. Thomas MB, Jaffe D, Choti MM, et al. Hepatocellular carcinoma: consensus -recommendations of the National Cancer Institute Clinical Trials Planning Meeting. J Clin Oncol 2010;28(25):3994–4005.
34. Pickles MD, Manton DJ, Lowry M, Turnbull LW. Prognostic value of pre-treatment DCE-MRI parameters in predicting disease free and overall survival for breast cancer patients undergoing neoadjuvant chemotherapy. Eur J Radiol 2009;71(3):498–505.
35. Flaherty KT, Rosen MA, Heitjan DF, et al. Pilot study of DCE-MRI to predict progression-free survival with sorafenib therapy

in renal cell carcinoma. Cancer Biol Ther 2008;7(4):496–501.

36. Shih TT, Hou HA, Liu CY, et al. Bone marrow angiogenesis magnetic resonance imaging in patients with acute myeloid leukemia: peak enhancement ratio is an independent predictor for overall survival. Blood 2009;113(14):3161–3167.

37. Chen BB, Hsu CY, Yu CW, et al. Dynamic contrast-enhanced MR imaging measurement of vertebral bone marrow perfusion may be indicator of outcome of acute myeloid leukemia patients in remission. Radiology 2011;258(3):821–831.

38. Jarnagin WR, Schwartz LH, Gultekin DH, et al. Regional chemotherapy for unresectable primary liver cancer: results of a phase II clinical trial and assessment of DCE-MRI as a biomarker of survival. Ann Oncol 2009;20(9):1589–1595.

39. Akisik MF, Sandrasegaran K, Bu G, Lin C, Hutchins GD, Chiorean EG. Pancreatic cancer: utility of dynamic contrast-enhanced MR imaging in assessment of antiangiogenic therapy. Radiology 2010;256(2):441–449.

40. Braren R, Altomonte J, Settles M, et al. Validation of preclinical multiparametric imaging for prediction of necrosis in hepatocellular carcinoma after embolization. J Hepatol 2011;55(5):1034–1040.

41. Roberts C, Issa B, Stone A, Jackson A, Waterton JC, Parker GJ. Comparative study into the robustness of compartmental modeling and model-free analysis in DCE-MRI studies. J Magn Reson Imaging 2006;23(4):554–563.

We thank Dr Lancelot and colleagues for their interest in our work. In their letter, they contest the difference in the numbers of patients in the study and control groups. In our study, liver gadolinium concentrations were evaluated in biopsy samples from living children. Biopsy is a highly invasive procedure for a pediatric transplant recipient. In our institution, the number of patients undergoing a liver biopsy without a GBCA-enhanced magnetic resonance (MR) examination is small, as the percentage of those with an uneventful posttransplant clinical history is also small. Ethically, it would be unacceptable to perform a biopsy on asymptomatic children. Inductively coupled plasma mass spectrometry is an expensive procedure for hospital budgets, but not for pharmaceutical companies that may wish to confirm or refute our results. Moreover, one of the studies cited by Dr Lancelot and colleagues (1) also compares two groups that greatly differ in numbers, with 19 patients in the study group and eight in the control group.

Second, our choice of a "LGC threshold of 0.1 μg/g, without scientific justification" was due to the lack of available reference values for LGC in the literature. We ask that colleagues of Guerbet kindly send us any missing bibliographic references.

Finally, Dr Lancelot and colleagues state that hematopoietic stem cell transplant recipients often present with deteriorated cardiac function due to iron overload (1). However, the study they cite only included patients with chronic or refractory anemia. Only one of our patients had chronic anemia, and that patient never received a transfusion. Hundreds of research papers have reported that children affected by thalassemia have a high rate of cardiac overload. Although liver iron overload is indeed frequent in patients who undergo hematopoietic stem cell transplantation, cardiac iron overload is rare (2). We do not believe that blood clots in the liver were the source of the retained gadolinium in these patients; regardless, histologic examination of liver ruled out the presence of thrombi.

The bibliographic references regarding cardiac function and hepatic veno-occlusive disease seem to be inconsistent and difficult to interpret. As clearly mentioned (3), the inclusion criteria included "healthy liver and renal function."

In conclusion, patients underwent GBCA-enhanced MR imaging only when other modalities did not provide exhaustive information about diagnosis. Although one can certainly object that our study was based on a limited number of patients, the results suggest the importance of fully investigating gadolinium retention in specific patient groups. It is our hope that Dr Lancelot and colleagues might, in the future, consider supporting investigations to better understand both the issue of gadolinium retention and the role of chelation therapy in managing the gadolinium accumulation.

Disclosures of Conflicts of Interest: N.M. disclosed no relevant relationships. **M.G.** disclosed no relevant relationships. **F.Z.** disclosed no relevant relationships. **A.S.** disclosed no relevant relationships. **R.S.** disclosed no relevant relationships. **D.Z.** disclosed no relevant relationships.

References

1. Seldrum S, Pierard S, Moniotte S, et al. Iron overload in polytransfused patients without heart failure is associated with subclinical alterations of systolic left ventricular function using cardiovascular magnetic resonance tagging. J Cardiovasc Magn Reson 2011;13:23.
2. Armand P, Sainvil MM, Kim HT, et al. Does iron overload really matter in stem cell transplantation? Am J Hematol 2012;87(6):569–572.
3. Maximova N, Gregori M, Zennaro F, Sonzogni A, Simeone R, Zanon D. Hepatic gadolinium deposition and reversibility after contrast agent–enhanced MR imaging of pediatric hematopoietic stem cell transplant recipients. Radiology DOI: 10.1148/radiol.2016152846. Published online June 8, 2016.

Erratum

Originally published in:
Radiology 2016;281(2):454–464
DOI: 10.1148/radiol.2016152659

Dynamic Contrast-enhanced MR Imaging of Advanced Hepatocellular Carcinoma: Comparison with the Liver Parenchyma and Correlation with the Survival of Patients Receiving Systemic Therapy

Bang-Bin Chen, Chao-Yu Hsu, Chih-Wei Yu, Po-Chin Liang, Chiun Hsu, Chih-Hung Hsu, Ann-Lii Cheng, Tiffany Ting-Fang Shih

Erratum in:
Radiology 2016;281(3):983
DOI:10.1148/radiol.2016164030

In an early online edition, page 461, Figure 2 legend should have read: For group 1 (blue line) versus group 2 (green line), median survival was 174 days and **193** days, respectively, and $P = .024$. This has been corrected online and in print.

Radiology

Errata

Originally published in:
Radiology 2016;279(1):322–323
DOI:10.1148/radiol.2016151739

Systemic Effects of Local Tumor Ablation: Oncogenesis and Antitumor Induced Immunity

Giovanni Mauri, Franco Orsi, Luca Maria Sconfienza

Erratum in:
Radiology 2017;283(3):923
DOI:10.1148/radiol.2017174015

The correct affiliation for Luca Maria Sconfienza should have been listed as follows: **Department of Radiology, IRCCS Policlinico San Donato, Piazza Malan 2, 20097 San Donato Milanese, Milan, Italy** and Department of Biomedical Sciences for Health, Università degli Studi di Milano, Milan, Italy.

Originally published in:
Radiology 2016;281(2):401–408
DOI: 10.1148/radiol.2016152514

Diagnostic Performance of Self-navigated Whole-Heart Contrast-enhanced Coronary 3-T MR Angiography

Yi He, Jianing Pang, Qinyi Dai, Zhanming Fan, Jing An, Debiao Li

Erratum in:
Radiology 2017;283(3):923
DOI:10.1148/radiol.2017174013

Page 401, the corresponding author should have been listed as follows**:** Address correspondence to **Z.F.** (e-mail: ***fanzm120@126.com***).

Originally published in:
Radiology 2016;281(2):454–464
DOI: 10.1148/radiol.2016152659

Dynamic Contrast-enhanced MR Imaging of Advanced Hepatocellular Carcinoma: Comparison with the Liver Parenchyma and Correlation with the Survival of Patients Receiving Systemic Therapy

Bang-Bin Chen, Chao-Yu Hsu, Chih-Wei Yu, Po-Chin Liang, Chiun Hsu, Chih-Hung Hsu, Ann-Lii Cheng, Tiffany Ting-Fang Shih

Erratum in:
Radiology 2017;283(3):923
DOI:10.1148/radiol.2017174012

A previously issued erratum *(http://dx.doi.org/10.1148/radiol.2016164030)* regarding this article was incorrect. Page 461, Figure 2 legend should read as follows: For group 1 (blue line) versus **group 3 (red line)**, median survival was 174 days and **110 days**, respectively, and $P = .024$. For group 2 **(green line)** versus group 3 (red line), median survival was 193 days and 110 days, respectively, and $P = .001$. No difference was observed between the two systemic therapy groups (group 1 vs group 2, median survival = 174 days vs 193 days, $P = .768$).